

DFTT 66/98  
LYCEN 98103

# The additive quark model revisited: hadron and photon induced cross-sections

P. Desgrolard<sup>(1)</sup>, M. Giffon<sup>(2)</sup>, E. Martynov<sup>(3)</sup>, E. Predazzi<sup>(4)</sup>.

<sup>(1,2)</sup>*Institut de Physique Nucléaire de Lyon, IN2P3-CNRS et Université Claude Bernard,  
43 boulevard du 11 novembre 1918, F-69622 Villeurbanne Cedex, France*

<sup>(3)</sup>*N.N. Bogoliubov Institute for Theoretical Physics, National Academy of Sciences of  
Ukraine, 252143, Kiev-143, Metrologicheskaja 14b, Ukraine*

<sup>(4)</sup>*Dipartimento di Fisica Teorica - Università di Torino and Sezione INFN di Torino, Italy*

**Abstract** The standard additive quark model and the ensuing counting rules are modified to take into account the quark-gluonic content of the Pomeron and of the secondary Reggeons. The result is that a much improved description of  $pp$ ,  $\pi p$ ,  $\gamma p$  and  $\gamma\gamma$  cross-sections is achieved.

## 1 Introduction

The Additive Quark Model (AQM)[1, 2, 3, 4] has provided for a long time a simple and successful model to describe, in particular, the main relations between the high energy cross-sections of different hadronic processes [5, 6]. Considering for example the pion-nucleon and the nucleon-nucleon interactions, one finds that the relation  $\sigma_{tot}^{\pi N}/\sigma_{tot}^{NN} = 2/3$  is in agreement with the available experimental data within an accuracy of a few percent. A linear dependence of the amplitudes on the number of quarks inside the scattered hadrons was confirmed on more fundamental grounds through QCD-like models [7, 8].

An interesting case to which we can apply (and test) the AQM lies into extending it to photon induced reactions because the data on these processes are now available up to quite high energies ( $\sqrt{s} \approx 200$  GeV for  $\gamma p$  and  $\sqrt{s} \approx 100$  GeV for  $\gamma\gamma$  inelastic cross-sections) [9, 10]. The three processes ( $pp$ ,  $\gamma p$  and  $\gamma\gamma$ ) are related via unitarity and factorization and this is the only set of related processes for each of which we have data. For the hadronic  $pp$ –,  $\pi p$ –,  $\pi\pi$ –reactions, the data on  $\pi\pi$ –interaction are in fact absent and  $\pi p$  total cross-sections are known only up to relatively low energies ( $\sqrt{s} < 30$  GeV).

Considering the above mentioned processes, first we show (Sect. 2) that the standard AQM does not describe the data with sufficiently high quality<sup>5</sup>. Next, In Sect. 3, we propose a modified AQM that takes into account the quark-gluonic content of the exchanged

---

<sup>1</sup>E-mail: desgrolard@ipnl.in2p3.fr

<sup>2</sup>E-mail: giffon@ipnl.in2p3.fr

<sup>3</sup>E-mail: martynov@bitp.kiev.ua

<sup>4</sup> E-mail: predazzi@to.infn.it

<sup>5</sup>We cannot compare the quality of our fit with those presented in some recent papers [11, 12] because their  $\chi^2$  is not given. Differences in their and our predictions for cross-sections at higher energies are discussed in Sect. 3

Reggeons. As a first try, we take into account Pomeron and  $f$ -Reggeon because they contribute to all amplitudes. The suggested modification provides a much improved agreement with the experimental data.

In order to make clear the content of our modification we will not consider here the scattering processes at  $t \neq 0$ . The parameterization of the scattering amplitudes at  $t \neq 0$  is much more complex than at  $t = 0$ . It will be the subject of a forthcoming paper.

## 2 The old additive quark model

### 2.1 The Pomeron

The traditional additive quark model treats the elastic scattering of two hadrons at high energy as Pomeron exchange between two quarks, one in each hadron. From the point of view of the quark-gluon picture, the Pomeron is represented by a gluon ladder with end points coupled with quark lines. The simplest diagram describing the main contribution to elastic hadron-hadron amplitude in the old AQM is exemplified in Fig. 1.

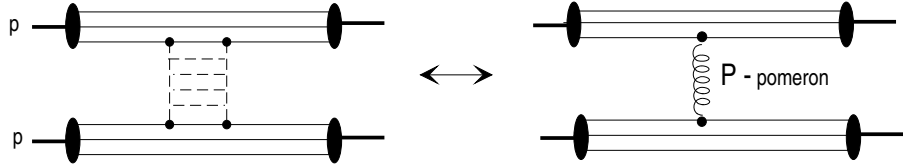


**Fig. 1.** The Pomeron diagrams for  $pp$ -scattering in the traditional additive quark model.

In accordance with AQM, when hadrons  $h_1$  and  $h_2$  (made of  $n_1$  and  $n_2$  quarks) are colliding, the Pomeron contribution to the elastic amplitude has the form

$$A_{\mathcal{P}}^{(h_1 h_2)}(s, t) = n_1 n_2 P_{h_1} P_{h_2} A_{\mathcal{P}}^{(qq)}(s_{h_1 h_2}, t) G_{\mathcal{P}}^{(h_1)}(t) G_{\mathcal{P}}^{(h_2)}(t) \quad (1)$$

where  $\sqrt{P_{h_i}}$  is the probability of finding the hadron  $h_i$  as a quark system,  $A_{\mathcal{P}}^{(qq)}(s, t)$  is the amplitude of elastic scattering of quarks due to the Pomeron and the squared energy  $s_{h_1 h_2}$  will be defined more precisely below ((9)).  $G_{h_i}(t)$  is the form factor of the hadron  $h_i$ ; it takes into account a redistribution of momenta of the quarks inside a hadron after the interaction of one of them with the Pomeron (each system of quarks should be preserved, after the interaction, as a hadron of the same kind). It is clear that  $G_{\mathcal{P}}^{(h_1)}(0) = G_{\mathcal{P}}^{(h_2)}(0) = 1$  at  $t = 0$ . In what follows we apply the traditional and the modified AQM to describe the total cross-sections

$$\sigma_{tot}(s) = 8\pi \Im m A(s, 0) \quad (2)$$

and the ratios of the real to the imaginary forward amplitudes

$$\rho(s) = \frac{\Re e A(s, 0)}{\Im m A(s, 0)}. \quad (3)$$

For the Pomeron contribution to the quark-quark scattering, we will consider two schemes. The first one is the Supercritical Pomeron (SCP) (*i.e.* a Pomeron with an intercept

larger than one, a variant of the Donnachie-Landshoff Pomeron (DLP)[13], but with a constant term added to reflect preasymptotic properties (this is nothing but a simple pole in the complex angular momentum plane with unit intercept)

$$A_{\mathcal{P}}^{(qq)}(s, 0) = ig_1^2[-\zeta + (-is/s_0)^{\alpha_{\mathcal{P}}(0)-1}] , \quad (4)$$

where  $s_0 = 1 \text{ GeV}^2$ .

The second model is the Dipole Pomeron (DP) model (see, for instance [14]), corresponding to a sum of a simple pole and a double  $j$ -pole with unit intercepts

$$A_{\mathcal{P}}^{(qq)}(s, 0) = ig_1^2[-\zeta + \ln(-is/s_0)] . \quad (5)$$

In both previous expressions the parameter  $\zeta$  is expected to be positive (from the fits to hadronic and  $\gamma p$  cross-sections [15, 16]).

As shown in [17], the Pomeron contribution at  $t \neq 0$  is more complicate than (1) because each term in (4) and (5) should be multiplied by *a priori* different vertex functions  $G(t)$ . Thus, at  $t \neq 0$ , (1) must be rewritten as

$$A_{\mathcal{P}}^{(h_1 h_2)}(s, t) = n_1 n_2 P_{h_1} P_{h_2} \sum_{i=1,2} A_{\mathcal{P}i}^{(qq)}(s_{h_1 h_2}, t) G_{\mathcal{P}i}^{(h_1)}(t) G_{\mathcal{P}i}^{(h_2)}(t), \quad (6)$$

where, generalizing (4) and (5),

$$A_{\mathcal{P}1}^{qq}(s, t) = -ig_1^2 \zeta (-is/s_0)^{\tilde{\alpha}_{\mathcal{P}}(t)-1}, \quad A_{\mathcal{P}2}^{qq}(s, t) = -ig_1^2 L(s, t), \quad \tilde{\alpha}_{\mathcal{P}}(0) = 1 \quad (7)$$

and

$$L(s, t) = (-is/s_0)^{\alpha_{\mathcal{P}}(t)-1}, \quad \alpha_{\mathcal{P}}(0) > 1 \quad \text{for SCP}, \quad (8)$$

$$L(s, t) = \ln(-is/s_0) (-is/s_0)^{\alpha_{\mathcal{P}}(t)-1}, \quad \alpha_{\mathcal{P}}(0) = 1 \quad \text{for DP} . \quad (8')$$

Generally speaking, the trajectories  $\alpha_{\mathcal{P}}(t)$  and  $\tilde{\alpha}_{\mathcal{P}}(t)$  can differ not only by their intercepts but also by their slopes.

At high energy, in the c.m. system, each hadron has the energy  $\sqrt{s/2}$  and, according to the AQM, each quark inside the hadron  $h_i$  has the energy  $\sqrt{s/2}/n_i$  (if  $n_i$  is the number of quarks comprised in the hadron  $h_i$ ). Thus, the energy of each pair of quarks (one from the hadron  $h_1$  and the other from the hadron  $h_2$ ) is

$$s_{h_1 h_2} = \left( \frac{\sqrt{s/2}}{n_1} + \frac{\sqrt{s/2}}{n_2} \right)^2 - \left( \frac{\sqrt{s/2}}{n_1} - \frac{\sqrt{s/2}}{n_2} \right)^2 = \frac{s}{n_1 n_2} . \quad (9)$$

There are nine ( $3 \times 3$ ) similar diagrams in  $pp$  scattering, contributing to the corresponding amplitudes

$$A_{\mathcal{P}i}^{(pp)}(s, t) = 9P_p^2 A_{\mathcal{P}i}^{(qq)}(s/9, t) (G_{\mathcal{P}i}^p(t))^2, \quad i = 1, 2 . \quad (10)$$

Considering also elastic  $\pi p$ -scattering with  $3 \times 2$  diagrams one can write

$$A_{\mathcal{P}i}^{(\pi p)}(s, t) = 6P_p P_{\pi} A_{\mathcal{P}i}^{(qq)}(s/6, t) G_{\mathcal{P}i}^p(t) G_{\mathcal{P}i}^{\pi}(t), \quad i = 1, 2 . \quad (11)$$

Let us focus now on  $\gamma$  induced processes for which the main Pomeron contributions (in the AQM) are shown in Fig. 2.

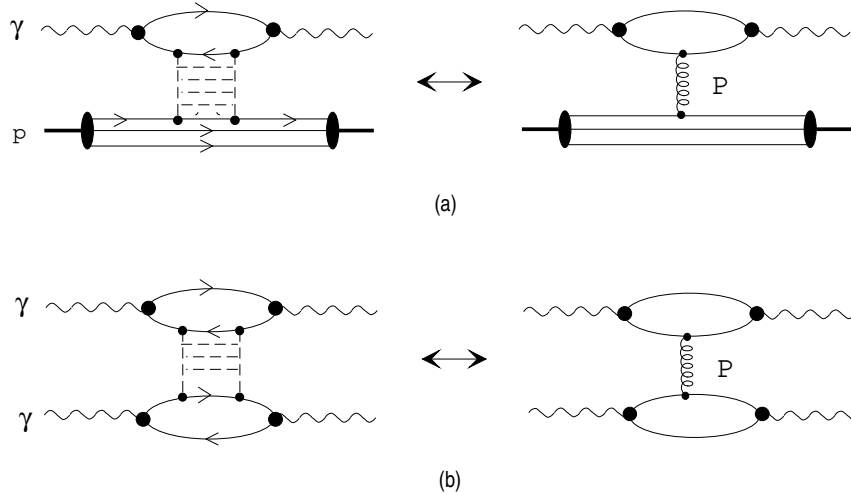


**Fig. 2.** The Pomeron diagrams for  $\gamma p$  (a) and  $\gamma\gamma$  (b) scattering in the old AQM.

The simplest approximation that describes the  $\gamma p$  elastic scattering as due to the Pomeron is

$$A_{\mathcal{P}_i}^{(\gamma p)}(s, t) = 6\alpha P_p A_{\mathcal{P}_i}^{(qq)}(s/6, t) G_{\mathcal{P}_i}^p(t) G_{\mathcal{P}_i}^\gamma(t), \quad i = 1, 2, \quad (12)$$

where  $\alpha = e^2/4\pi \approx 1/137$  is the fine structure constant. (12) takes into account the  $\gamma q\bar{q}$  vertices in the  $q\bar{q}$  loop at the upper block of the diagram of Fig. 2a. Similarly, the relevant  $\gamma\gamma$  amplitude (Fig. 2b) has the form

$$A_{\mathcal{P}_i}^{(\gamma\gamma)}(s, t) = 4\alpha^2 A_{\mathcal{P}_i}^{(qq)}(s/4, t) (G_{\mathcal{P}_i}^\gamma(t))^2, \quad i = 1, 2. \quad (13)$$

It is, however, more realistic to consider a different picture for  $\gamma p$  and  $\gamma\gamma$  diagrams. In accordance with the Vector Meson Dominance (VDM) model, the photon is transformed into a vector meson which, after interacting with the Pomeron, comes back to a photon state. Thus, we replace  $\alpha \rightarrow P_\gamma$  in (12),(13) where  $\sqrt{P_\gamma}$  describes the transition of a  $\gamma$  into a pair  $q\bar{q}$  (for instance, via a vector meson).

## 2.2 Secondary Reggeons

At the presently attainable (subasymptotic) squared energy  $s$ , beside the Pomeron, one should retain also the contribution of other Reggeons ( $f, \rho, \omega$  etc) to the elastic amplitudes. It is usually assumed that they are added to the Pomeron so that the amplitude becomes

$$A^{(h_1 h_2)}(s, t) = A_{\mathcal{P}}^{(h_1 h_2)}(s, t) + n_1 n_2 P_{h_1} P_{h_2} \sum_R A_R^{(qq)}(s_{h_1 h_2}, t) G_R^{(h_1)}(t) G_R^{(h_2)}(t), \quad (14)$$

where the Pomeron amplitude is detailed in the preceding section and the sum over  $R$  runs over all Reggeons contributing to the given process. In what follows, we will consider  $pp$ ,  $\pi p$ ,  $\gamma p$  and  $\gamma\gamma$  scattering at  $\sqrt{s} \geq 4$  GeV and  $t = 0$ . Therefore, only  $f$  and  $\omega$  will contribute to  $p^\mp p$  processes (here and in what follows  $p^- \equiv \bar{p}$ ,  $p^+ \equiv p$ ),  $f$  and  $\rho$  to  $\pi^\mp p$  and  $f$  to  $\gamma p$  and  $\gamma\gamma$ . For the secondary Reggeons we take the standard form

$$A_f^{(qq)}(s, t) = ig_f^2 \left( -is/s_0 \right)^{\alpha_f(t)-1}, \quad (15)$$

$$A_{\omega}^{(qq)}(s, t) = g_{\omega}^2 \left( -is/s_0 \right)^{\alpha_{\omega}(t)-1}, \quad (16)$$

$$A_{\rho}^{(qq)}(s, t) = g_{\rho}^2 \left( -is/s_0 \right)^{\alpha_{\rho}(t)-1}. \quad (17)$$

### 2.3 Complete AQM amplitude

Collecting all the previous results, the relevant amplitudes at  $t = 0$ <sup>6</sup> in the old additive quark model for the four cases under investigation are

$$A^{(p\bar{p})}_{pp}(s, 0) = 9P_p^2 \left[ A_{\mathcal{P}}^{(qq)}(s/9, 0) + A_f^{(qq)}(s/9, 0) \pm A_{\omega}^{(qq)}(s/9, 0) \right], \quad (18)$$

$$A^{(\pi^{\pm} p)}_{\pi^{\pm} p}(s, 0) = 6P_{\pi}P_p \left[ A_{\mathcal{P}}^{(qq)}(s/9, 0) \pm A_{\rho}^{(qq)}(s/6, 0) \right], \quad (19)$$

$$A^{(\gamma p)}(s, 0) = 6P_{\gamma}P_p \left[ A_{\mathcal{P}}^{(qq)}(s/6, 0) + A_f^{(qq)}(s/6, 0) \right], \quad (20)$$

$$A^{(\gamma\gamma)}(s, 0) = 4P_{\gamma}^2 \left[ A_{\mathcal{P}}^{(qq)}(s/4, 0) + A_f^{(qq)}(s/4, 0) \right] \quad (21)$$

where the Pomeron quark-quark amplitude  $A_{\mathcal{P}}^{(qq)}$  is defined by (4) or (5) and the Reggeon quark-quark amplitudes  $A_R^{(qq)}$  are written in (15)-(17).

### 2.4 Comparison of the data with the old AQM

The above amplitudes have been fitted to the experimental data [9, 10, 19, 20] at  $\sqrt{s} \geq 4$  GeV (totally 434 points) listed in Table 1.

We did not include in our data set a few points on  $\rho^{\pi^{\pm} p}$  because of their large errors. They do not lead to any noticeable change in the values of parameters and in the behaviour of the curves.

Without any loss of generality we can take  $P_p = 1$  in the previous equations since this acts as an overall multiplication parameter in the fit.

We compare three models of Pomeron:

- DLP : Supercritical Pomeron with  $\zeta = 0$  in (4) (which is close to the Pomeron in [13]).
- SCP : Supercritical Pomeron with free  $\zeta$ .
- DP : Dipole Pomeron with  $\alpha_{\mathcal{P}}(0) = 1$ .

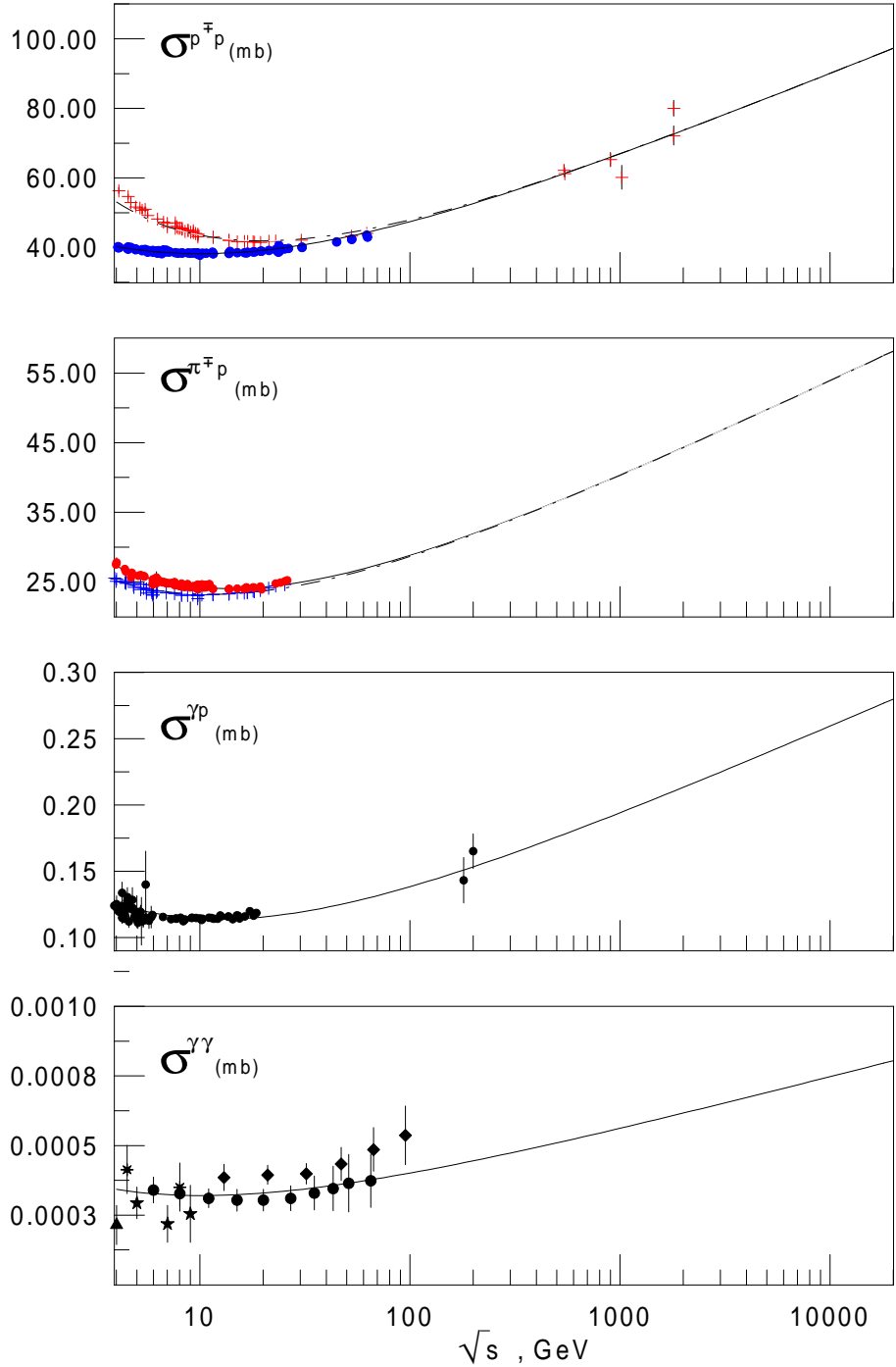
The description of these data in all models are comparable to each other; the  $\chi^2$  for cases b) and c),  $\chi^2/d.o.f. \approx 3.04$ , is very close to that of case a)  $\chi^2/d.o.f. \approx 3.09$ . It is interesting to note, nevertheless, that, if the parameter  $\zeta$  is allowed to be free, the intercept of the Supercritical Pomeron tends to 1 and the other parameters approach those obtained in the Dipole Pomeron model. The same situation was observed in [15], where these models were compared with all the data on the meson-nucleon and nucleon-nucleon cross-sections and  $\rho$ -s. We will come back to these questions below when discussing the modified AQM. In Figs. 3,4 we present the curves corresponding to the Dipole Pomeron (case c)). The curves for both variants of SCP are very close to the DP curves.

---

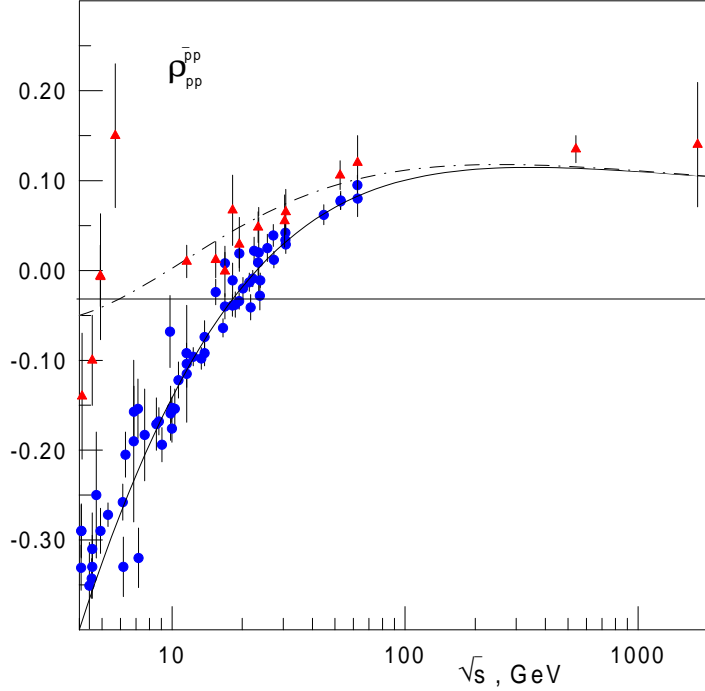
<sup>6</sup> This is all we need for total cross-sections.

Table 1: Number of experimental data points used in the fit to the cross-sections and  $\rho$ -values of the various processes

Observable	$\sigma_{pp}$	$\sigma_{\bar{p}p}$	$\sigma_{\pi^- p}$	$\sigma_{\pi^+ p}$	$\sigma_{\gamma p}$	$\sigma_{\gamma\gamma}$	$\rho_{pp}$	$\rho_{\bar{p}p}$
Number of points	85	51	49	83	68	17	64	17



**Fig. 3.** Total cross-sections described in old AQM with the Dipole Pomeron.



**Fig. 4.** Ratio of the forward real to imaginary part for  $pp$  and  $\bar{p}p$  scattering in the old AQM with the Dipole Pomeron.

### 3 Modification of the additive quark model

#### 3.1 Pomeron

In the spirit of the QCD-like picture, the Pomeron (a gluonic ladder as a first approximation) has at least four gluonic edges coupled with quark lines. Besides the diagrams of Fig.1,2 however, additional terms may contribute to the amplitudes. They correspond to diagrams in which the Pomeron line is coupled with two quark lines rather than with one only, leading to a modified additive quark model (MAQM). Examples of such diagrams are shown in Fig. 5. The cheapest price to pay for this generalization is an additional coupling constant describing the vertex Pomeron - two quark lines. This constant can be determined from the fit to experimental data and can be considered as a measure of the deviation between the new counting rules and the old ones.

We would like to note here that in spite of an apparent analogy, the right hand side Pomeron diagrams in Fig. 5 (as well as in the other Figures) are not exactly the ladder diagrams, shown on the left hand side of Fig. 5. The latter, in fact, assume that each vertex of the gluonic ladder of the Pomeron couples to the hadron via lines of individual quarks only while the diagrams on the right hand side of Fig. 5 do not exclude that a soft Pomeron can be exchanged between single quarks and pair of quarks (not necessarily a diquark; all possible states of this pair of quarks are "hidden" in the new coupling constant) or between two pairs of quarks.

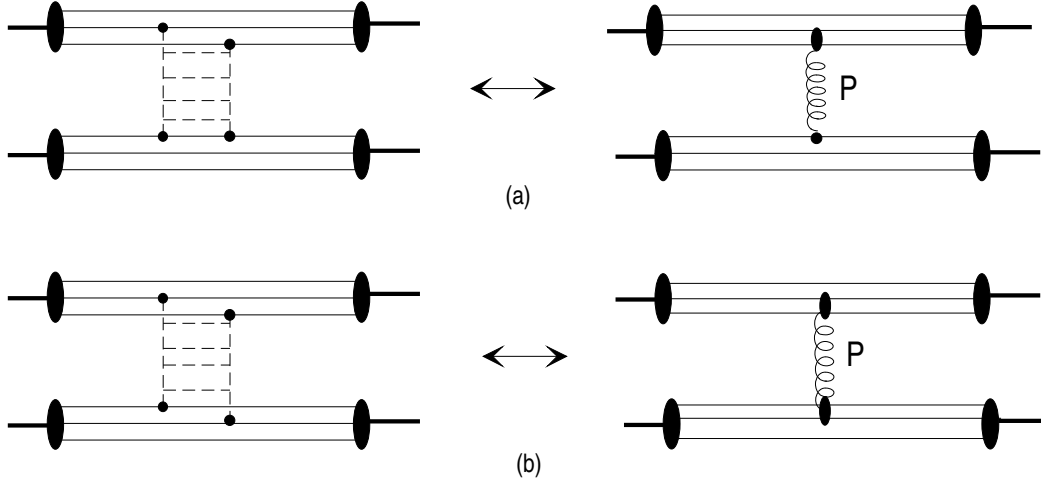


**Fig. 5.** Additional Pomeron diagrams in the modified AQM (examples).

As it is well known, a soft Pomeron satisfying unitarity does not reduce to ladder diagrams. There is a difference between a two-gluon approximation to the Pomeron (used for example in [7, 8]) and a soft Pomeron which is certainly a more complicate object than a gluonic ladder. Because a calculable scheme for a soft Pomeron is not known, we are forced to rely on phenomenological models.

Taking into account all possible diagrams that can contribute to each case, we redefine the Pomeron contributions (10-13) in the following form (once again, it is sufficient to write all amplitudes at  $t = 0$  because our modification concerns the counting rules rather than the form of the amplitudes; a generalization to  $t \neq 0$  is, however, immediate from the previous Section)

$p^\mp p$ -interaction:

$$A_{\mathcal{P}}^{(pp)}(s, 0) = 9P_p^2[A_{\mathcal{P}}^{(1)}(s/9, 0) + 2A_{\mathcal{P}}^{(2)}(2s/9, 0) + A_{\mathcal{P}}^{(3)}(4s/9, 0)], \quad (22)$$

$\pi^\mp p$ -interaction:

$$A_{\mathcal{P}}^{(\pi p)}(s, 0) = 3P_\pi P_p[2A_{\mathcal{P}}^{(1)}(s/6, 0) + 3A_{\mathcal{P}}^{(2)}(s/3, 0) + A_{\mathcal{P}}^{(3)}(2s/3, 0)], \quad (23)$$

$\gamma p$ -interaction:

$$A_{\mathcal{P}}^{(\gamma p)}(s, 0) = 3P_\gamma P_p[2A_{\mathcal{P}}^{(1)}(s/6, 0) + 3A_{\mathcal{P}}^{(2)}(s/3, 0) + A_{\mathcal{P}}^{(3)}(2s/3, 0)], \quad (24)$$

$\gamma\gamma$ -interaction:

$$A_{\mathcal{P}}^{(\gamma\gamma)}(s, 0) = P_\gamma^2[4A_{\mathcal{P}}^{(1)}(s/4, 0) + 4A_{\mathcal{P}}^{(2)}(s/2, 0) + A_{\mathcal{P}}^{(3)}(s, 0)], \quad (25)$$

where we have defined

$$A_{\mathcal{P}}^{(1)}(s, 0) = i[-\eta_1^2 + g_1^2 L(s)], \quad (26)$$

$$A_{\mathcal{P}}^{(2)}(s, 0) = i[-\eta_1\eta_2 + g_1 g_2 L(s)], \quad (27)$$

$$A_{\mathcal{P}}^{(3)}(s, 0) = i[-\eta_2^2 + g_2^2 L(s)]. \quad (28)$$

Here  $L(s) = (-is/s_t)^{\alpha_{\mathcal{P}}(0)-1}$  in the SCP model and  $L(s) = \ln(-is/s_0)$  in the DP model (and  $\eta_1, \eta_2$  are constants).

Each Pomeron term  $A_{\mathcal{P}}^{(i)}(s, 0)$ ,  $i = 1, 3$  is the sum of two contributions : the first corresponds to a double  $j$ -pole (with couplings  $g_1, g_2$  describing the vertices with one and two quarks as indicated in Fig. 1 and Fig. 5) and the second corresponds to a simple pole (with couplings  $\eta_1$  and  $\eta_2$ ). As already noted in Sect.2.1 a negative contribution of the simple pole is suggested from fitting the hadronic amplitudes to the data; this is why we have a negative sign in front of the  $\eta$ 's in (26)-(28). The available data, however, are not sufficient to determine four coupling constants  $(g_k, \eta_k)$ ; for this reason we consider the simpler case in which

$$\eta_1^2/g_1^2 = \eta_2^2/g_2^2 = \zeta.$$

As follows from unitarity, the total cross-sections for  $nn$ ,  $\pi n$  and  $\pi\pi$  interactions (by cross-section  $nn$  and  $\pi n$  we mean here  $\sigma_{nn} = (\sigma_{pp} + \sigma_{\bar{p}p})/2$  and  $\sigma_{\pi n} = (\sigma_{\pi^+p} + \sigma_{\pi^-p})/2$ ) should satisfy at asymptotic energies the factorization relation [18]

$$\sigma_{\pi n}^2 = \sigma_{\pi\pi}\sigma_{nn}.$$

One can check that this relation holds also in the MAQM if the constant terms in (26)-(28) are neglected. But the well known relation,  $\sigma_{\pi n}/\sigma_{nn} = 3/2$ , does not hold exactly in the MAQM. For the Dipole Pomeron ( $L(s) = \ln(-is/s_0)$ ) this is modified into

$$\sigma_{\pi n}/\sigma_{nn} = \sigma_{\pi\pi}/\sigma_{\pi n} \approx \frac{2P_\pi}{3P_p} \left(1 - \frac{1}{2} \frac{g_1}{g_2}\right),$$

if  $g_1/g_2 \ll 1$  as it is expected (and confirmed by data, see below). The same relations are valid (under the replacement  $\pi \rightarrow \gamma$  in the indices) for  $nn$ ,  $\gamma n$  and  $\gamma\gamma$  processes.

### 3.2 Secondary Reggeons.

While the Pomeron is mostly a gluonic state, which can be coupled with any quark independently of its flavour, the Reggeons must be considered as  $q\bar{q}$ -states (see Fig. 6). Concerning the  $f$ -Reggeon (as well as other Reggeons with vacuum quantum numbers) which, being neutral is a mixing of  $u\bar{u}$  and  $d\bar{d}$ , not of  $u\bar{d}$  and  $d\bar{u}$  states (we ignore here the small contribution of other  $q\bar{q}$  states to the  $f$ -meson and, consequently, to the  $f$ -Reggeon), its diagrammatic structure within our approach is shown in Fig. 6.

Thus, for the  $pp$ -diagram the  $f$ -Reggeon can couple only to quarks with identical flavour. There are four diagrams where the  $f$ -Reggeon couples to  $u$ -quarks and one to  $d$ -quarks. The summation leads to 5  $f$ -Reggeon diagrams in  $pp$ -scattering instead of 9 diagrams for the Pomeron and for the  $f$ -Reggeon in the old AQM. One obtains

$$A_f^{(pp)}(s, 0) = 5P_p^2 A_f^{(qq)}(s/9, 0). \quad (29)$$

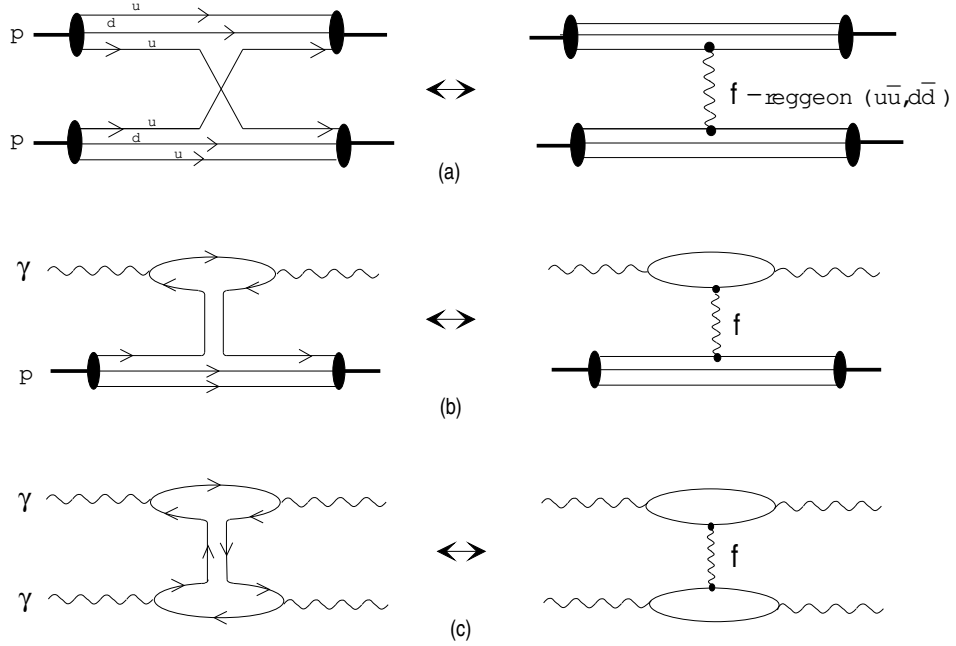


**Fig. 6.** The  $f$ –Reggeon diagrams for  $pp$ ,  $\gamma p$  and  $\gamma\gamma$  scattering.

Similarly, for the  $\pi p$  diagrams

$$A_f^{(\pi p)}(s, 0) = 3P_\pi P_p A_f^{(qq)}(s/6, 0). \quad (30)$$

The same couplings apply to  $\gamma p$  diagrams. The upper loop in Fig. 6b can contain either  $u\bar{u}$  or  $d\bar{d}$  quarks with  $1/2$  probability for each case. Therefore, there are  $2 \cdot 2 \cdot \frac{1}{2} = 2$  terms for the  $u$ –loop and  $2 \cdot \frac{1}{2} = 1$  term for the  $d$ –loop leading to

$$A_f^{(\gamma p)}(s, 0) = 3P_\gamma P_p A_f^{(qq)}(s/6, 0). \quad (31)$$

Performing a similar counting for the  $\gamma\gamma$  amplitude, we obtain

$$A_f^{(\gamma\gamma)}(s, 0) = 2P_\gamma^2 A_f^{(qq)}(s/4, 0). \quad (32)$$

The crossing-odd  $\omega$ –Reggeon contributes only to the  $pp$  and  $\bar{p}p$  amplitudes and we have

$$A_\omega^{(pp)}(s, 0) = 5P_p^2 A_\omega^{(qq)}(s/9, 0). \quad (33)$$

Similarly, the  $\rho$  contribution to the  $\pi^\mp p$  amplitudes leads to

$$A_\rho^{(pp)}(s, 0) = 3P_p^2 A_\rho^{(qq)}(s/6, 0). \quad (34)$$

Strictly, we should consider two contributions since, in addition to the previous coupling with two quark lines with the same flavors ( $uu$  or  $dd$ ), we may also have another coupling with two quark lines with different flavors ( $ud$ ), because all secondary Reggeons with vacuum quantum numbers are mixed states of  $u\bar{u}$  and  $d\bar{d}$  (we neglect harder flavors). We can describe such a transition from a  $u\bar{u}$  state to a  $d\bar{d}$  one by a new constant (see Fig. 7).

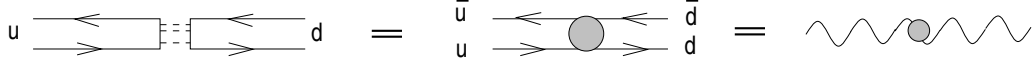


**Fig. 7.** Mixing of  $u\bar{u}$  and  $d\bar{d}$  states in a secondary Reggeon.

For simplicity, we assume that this new contribution is given by multiplying the old  $R$ -Reggeon term by a constant  $\lambda_R$ . Note, however, that the counting rules for this new terms are different from those which couple identical quarks. Let us write down the complete  $f$ -Reggeon contribution to the amplitudes.

$pp$ -interaction:

$$A_f^{(pp)}(s, 0) = P_p^2 [5A_{f1}^{(qq)}(s/9, 0) + 4A_{f2}^{(qq)}(s/9, 0)] = P_p^2 (5 + 4\lambda_f) A_f^{(qq)}(s/9, 0), \quad (35)$$

$\pi p$ -interaction:

$$A_f^{(\pi p)}(s, 0) = 3P_\pi P_p [A_{f1}^{(qq)}(s/6, 0) + A_{f2}^{(qq)}(s/6, 0)] = 3P_\pi P_p (1 + \lambda_f) A_f^{(qq)}(s/6, 0), \quad (36)$$

$\gamma p$ -interaction:

$$A_f^{(\gamma p)}(s, 0) = 3P_\gamma P_p [A_{f1}^{(qq)}(s/6, 0) + A_{f2}^{(qq)}(s/6, 0)] = 3P_\gamma P_p (1 + \lambda_f) A_f^{(qq)}(s/6, 0), \quad (37)$$

$\gamma\gamma$ -interaction:

$$A_f^{(\gamma\gamma)}(s, 0) = 2P_\gamma^2 [A_{f1}^{(qq)}(s/4, 0) + A_{f2}^{(qq)}(s/4, 0)] = 2P_\gamma^2 (1 + \lambda_f) A_f^{(qq)}(s/4, 0) \quad (38)$$

where

$$A_{f1}^{(qq)}(s, 0) \equiv A_f^{(qq)}(s, 0)$$

and

$$A_{f2}^{(qq)}(s, 0) \equiv \lambda_f A_f^{(qq)}(s, 0).$$

The value of  $\lambda_f$  should be determined from a fit to the experimental data. Note that if  $\lambda_f = 1$  one comes back to the old counting rules for the  $f$ -Reggeon.

The  $\omega$  and  $\rho$  Reggeon contributions are easily derived from the above expressions. It should be noted that the counting rules for these Reggeons are unimportant in our fit because we consider one by one the processes to which they contribute. Namely,  $\omega$  contributes only to  $pp$  and  $\rho$  contributes only to  $\pi p$  amplitudes. Thus, it is sufficient to write them in the old AQM form.

### 3.3 Complete MAQM amplitudes

Summarizing the results of the new counting rules, the final expressions for the  $t = 0$  amplitudes of the reactions under investigation in the Modified Additive Quark Model are:

1.  $pp$  and  $\bar{p}p$  (or  $p^\mp p$ ) amplitudes

$$\begin{aligned} A^{p\mp p}(s, 0) = & P_p^2 \{9[A_{\mathcal{P}}^{(1)}(s/9, 0) + 2A_{\mathcal{P}}^{(2)}(2s/9, 0) + A_{\mathcal{P}}^{(3)}(4s/9, 0)] \\ & + (5 + 4\lambda_f) A_f(s/9, 0) \pm 9A_\omega(s/9, 0)\}, \end{aligned} \quad (39)$$

2.  $\pi^- p$  and  $\pi^+ p$  amplitudes

$$\begin{aligned} A^{\pi^\mp p}(s, 0) &= P_\pi P_p \{3[2A_\mathcal{P}^{(1)}(s/6, 0) + 3A_\mathcal{P}^{(2)}(s/3, 0) + A_\mathcal{P}^{(3)}(2s/3, 0)] \\ &+ 3(1 + \lambda_f)A_f(s/6, 0) \pm 6A_\rho(s/6, 0)\}, \end{aligned} \quad (40)$$

3.  $\gamma p$  amplitude

$$\begin{aligned} A^{\gamma p}(s, 0) &= P_\gamma P_p \{3[2A_\mathcal{P}^{(1)}(s/6, 0) + 3A_\mathcal{P}^{(2)}(s/3, 0) + A_\mathcal{P}^{(3)}(2s/3, 0)] \\ &+ 3(1 + \lambda_f)A_f(s/6, 0)\}, \end{aligned} \quad (41)$$

4  $\gamma\gamma$  amplitude

$$\begin{aligned} A^{\gamma\gamma}(s, 0) &= P_\gamma^2 \{4A_\mathcal{P}^{(1)}(s/4, 0) + 4A_\mathcal{P}^{(2)}(s/2, 0) + A_\mathcal{P}^{(3)}(s, 0) \\ &+ 2(1 + \lambda_f)A_f(s/4, 0)\}. \end{aligned} \quad (42)$$

### 3.4 Comparison of the data with the Modified AQM

We now proceed to utilize the same set of data used previously (Table 1) to perform the same fit for the MAQM. The values of the free parameters for the three models of Pomeron considered are given in Table 2. It is evident that the Modified Additive Quark Model leads to a better description of the data: the value of  $\chi^2/d.o.f.$  decreases from 3.04 to 1.78 for cases b) and c) and to 2.03 for case a). The behaviour of  $\sigma_{tot}$  and  $\rho$  is shown in the Figs. 8,9 (once again, we confine ourselves to plot the curves only for the case of the Dipole Pomeron). The improvement for  $\sigma^{p^\mp p}$  and  $\rho^{p^\mp p}$  is quite visible. The improvement for  $\pi p$  and  $\gamma p$  is less clearly visible in the figures but exists.

The first conclusion is, therefore, that the modified AQM agrees with data noticeably better than the old AQM does.

We also note that the Supercritical Pomeron with an additional constant term (i.e. with  $\zeta = \eta_1^2/g_1 = \eta_2^2/g_2 \neq 0$  in (26-8)) is very close to the Dipole Pomeron. As a matter of fact, given the small value of  $\epsilon$  obtained from the fit (see Table 2),  $\epsilon = \alpha_\mathcal{P}(0) - 1 \approx 0.0005$ , one can write the Supercritical Pomeron contribution, for instance to the  $pp$  amplitude, in a form undistinguishable in practice from the Dipole Pomeron case

$$A_\mathcal{P}^{pp} = ig_1^2[-\zeta + (-is/s_0)^\epsilon] \approx ig_1^2[-\zeta + 1 + \epsilon \ln(-is/s_0)] = i\tilde{g}_1^2[-\tilde{\zeta} + \ln(-is/s_0)]$$

where  $\tilde{g}_1^2 = \epsilon g_1^2$ ,  $\tilde{\zeta} = (\zeta - 1)/\epsilon$ . From the parameters given in Table 2, we find  $\tilde{g}_1 \approx 0.31$ ,  $\tilde{\zeta} \approx 3.02$  which are close to the corresponding parameters of the Dipole Pomeron. The parameters of the other Reggeons are also close to those obtained for the Dipole Pomeron model.

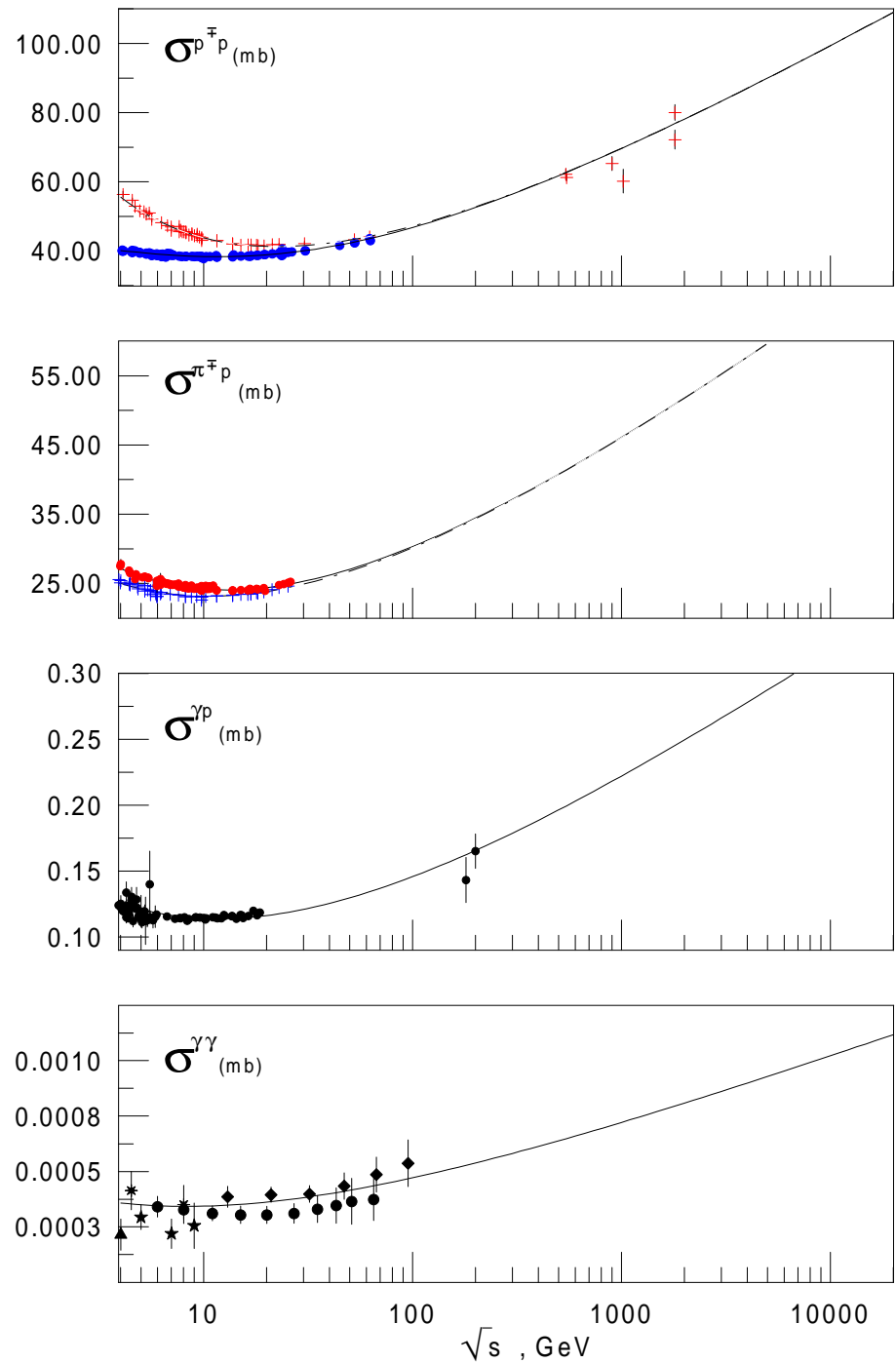


**Fig. 8.** Total cross-sections described in the MAQM with the Dipole Pomeron.

Table 2: The values of parameters obtained in MAQM for three variants of Pomeron .

Parameters	SCP, $\zeta = 0$	SCP, $\zeta \neq 0$	DP
$g_1$ (GeV $^{-1}$ )	0.583	13.346	0.317
$g_2$ (GeV $^{-1}$ )	-0.079	-0.826	-0.024
$\alpha_P(0)$	1.101	1.0005	1.0 (fixed)
$\zeta$	0.0 (fixed)	1.003	3.399
$P_p$	1.0 (fixed)	1.0 (fixed)	1.0 (fixed)
$P_\pi$	0.848	0.925	0.919
$P_\gamma$	0.0041	0.0044	0.0044
$g_f$ (GeV $^{-1}$ )	0.822	1.120	1.112
$\alpha_f(0)$	0.661	0.803	0.810
$\lambda_f$	0.094	0.343	0.439
$g_\omega$ (GeV $^{-1}$ )	0.396	0.395	0.395
$\alpha_\omega(0)$	0.403	0.418	0.421
$g_\rho$ (GeV $^{-1}$ )	0.230	0.221	0.222
$\alpha_\rho(0)$	0.592	0.586	0.587
$\chi^2/\text{d.o.f.}$	2.025	1.784	1.780

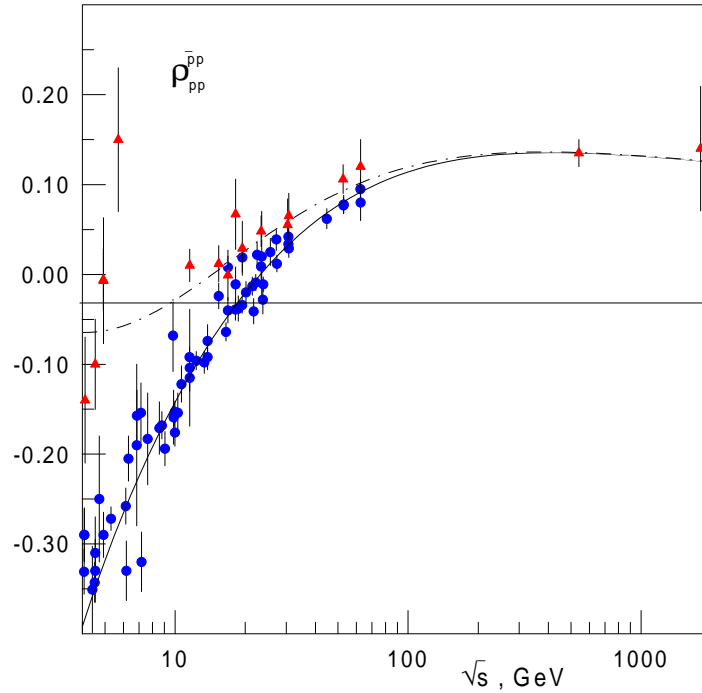


**Fig. 9.** Ratio of the forward real to imaginary part for  $pp$  and  $\bar{p}p$  scattering in the MAQM with the Dipole Pomeron.

From this point of view, we can say that the Dipole Pomeron is preferable to the Super-critical Pomeron. From the theoretical point of view it will never violate the Froissart-Martin

unitarity bound, and from the phenomenological point of view it has one parameter less (because  $\alpha_P(0) = 1$ ).

Our analysis of data does not support the conclusion drawn in [11] about  $\sigma_{inel}^{\gamma\gamma}$ , that the preliminary OPAL are doubtful and that the VMD selects the L3 data<sup>7</sup>. One can see from Fig. 8 that the theoretical curve goes precisely between the points of these two groups. Generally, we predict higher values of  $\sigma^{\gamma p}$  and  $\sigma^{\gamma\gamma}$  than given in [11], but smaller than those obtained for these cross-sections in the mini-jets model [21].

## 4 Conclusion

Our main result is the following. A proper account of the quark-gluonic content of Pomeron and  $f$ -Reggeon leads to slightly modified counting rules for the quark-quark amplitudes when constructing the hadron-hadron, photon-hadron and photon-photon amplitudes. The additional new Pomeron terms give  $\approx 10\%$  of the whole Pomeron contribution, while for  $f$ -Reggeon the new term contributes  $\approx 30\%$  of the whole  $f$ -Reggeon component.

The important role of these terms is confirmed by the analysis of the data on the total cross-sections of hadron and photon induced processes. They lead to a decrease of the  $\chi^2/d.o.f.$  by approximately 40%, thus improving the description of the data.

In conclusion, we have shown that a modification of the additive quark model in which one takes into proper account the contribution of more diagrams leads to a quantitatively better fit of all available  $t = 0$  data. While not dramatic, this improvement gives us hope that the MAQM will give a substantially better result when the model will be applied outside  $t = 0$ . This we plan to do in the near future.

**Acknowledgements.** Financial support is gratefully acknowledged from the IN2P3 of France and from the INFN and the MURST of Italy. E.M. wishes also to thank the Theory groups of the Universities of Lyon and Torino for their hospitality.

## References

- [1] E.M. Levin and L.L. Frankfurt, *Pisma ZhETP*, **3** (1965) 105.
- [2] H.J. Lipkin and F. Scheck, *Phys. Rev. Lett.* **16** (1966) 71.
- [3] J.J.J. Kokkedee and L. Van Hove, *Nuovo Cim.*, **42A** (1966) 711.
- [4] J.J.J. Kokkedee, *The Quark model*, W.A. Benjamin, Inc., New York, 1969.
- [5] V.V. Anisovich, Yu.M. Shabelsky and V.M. Shekhter, *Nucl.Phys.* **B133** (1978) 477.
- [6] E.S. Martynov, in *Proceedings of the Workshop on "DIQUARKS II"*. 2-4 November 1992, Torino Italy, 1992.
- [7] J.F. Gunion and D.E. Soper, *Phys. Rev.* **D15** (1977) 2617.

---

<sup>7</sup>The predictions of Ref.[11] are based on the counting rules of the old AQM, which should be modified as we have argued.

- [8] E.M. Levin and M.G. Ryskin, *Yad. Fiz.* (Sov. Nucl. Phys.). **34** (1981) 1114.
- [9] M. Derrick *et al.*, ZEUS Collaboration, *Zeit. Phys. C* **63** (1994) 391; S. Aids *et al.*, H1 Collaboration, *Zeit. Phys. C* **69** (1995) 27; Data for  $\gamma p$  cross-sections at low energies can be found, for instance, in the Durham Data Base (<http://cpt1.dur.ac.uk/HEPDATA>).
- [10] Ch. Berger *et al.*, PLUTO Collaboration, *Phys. Lett. B* **149** (1984) 421; H. Aihara *et al.* TCP/2 $\gamma$  Collaboration, *Phys. Rev. D* **41** (1990) 2667; S.E. Baru *et al.*, MD-1 Collaboration, *Zeit. Phys. C* **53** (1992) 219; M. Acciari *et al.*, L3 Collaboration, *Phys. Lett. B* **408** (1997) 450; F. Wäckerle, "Total Hadronic Cross-section for Photon-Photon Interactions at LEP", Preprint Freiburg-EHEP-97-17, 1997.
- [11] M.M. Block *et al.*, [hep-ph/9809403](http://arxiv.org/abs/hep-ph/9809403), 1998, *Phys. Rev. D* **58** (1998) 17503.
- [12] A. Donnachie, R.G. Dosch and M. Rueter, [hep-ph/9810206](http://arxiv.org/abs/hep-ph/9810206), 1998.
- [13] A. Donnachie and P. Landshoff, *Phys. Lett. B* **296** (1992) 227.
- [14] L.L. Jenkovszky, *Fortschr. Phys.* **34** (1986) 702; M. Bertini *et al.*, *Rivista Nuovo Cim.* **19** (1996) 1.
- [15] P. Desgrolard *et al.*, *Nuovo Cim.* **107A** (1994) 637.
- [16] P. Desgrolard, A.I. Lengyel and E.S. Martynov, *Nuovo Cim.* **110A** (1997) 251.
- [17] P. Desgrolard, A.I. Lengyel and E.S. Martynov, *Eur. Phys. Jour. C*, *in press*.
- [18] See, for example, P.D.B. Collins, *An Introduction to Regge Theory and High Energy Physics*, Cambridge University Press, 1977.
- [19] For  $pp$  and  $\bar{p}p$  data on  $\sigma_{tot}$  and  $\rho$  see, for example, S.M. Pruss, in *Frontiers in Strong Interactions, VII Blois Workshop on Elastic and Diffraction Scattering, Chateau de Blois, France, June 1995*, edited by P. Chiappetta, M. Haguenauer and J. Tran Thanh Van (Editions Frontières 1996), p.3, and references therein; Durham Data Base (<http://cpt1.dur.ac.uk/HEPDATA>).
- [20] Data on  $\pi p$  total cross-sections can be found in the Durham Data Base (<http://cpt1.dur.ac.uk/HEPDATA>).
- [21] A. Corsetti, R.M. Godbole and G. Pancheri, *Phys.Lett. B* **435** (1998) 441.